Materials Science Forum *Online: 2018-12-26*
ISSN: 1662-9752, Vol. 941, pp 236-244
doi:10.4028/www.scientific.net/MSF.941.236

VC-Precipitation Kinetics Studied by Small-Angle Neutron Scattering in Nano-Steels

Chrysoula Ioannidou[1,a*], Zaloa Arechabaleta[1,b,§], Arjan Rijkenberg[2,c], Robert M. Dalgliesh[3,d], Ad A. van Well[4,e] and S. Erik Offerman[1,f]

[1]Department of Materials Science and Engineering, Delft University of Technology, Mekelweg 2, 2628 CD Delft, The Netherlands

[2]Tata Steel, 1970 CA IJmuiden, The Netherlands

[3]STFC, ISIS, Rutherford Appleton Laboratory, Chilton, Oxfordshire, OX11 0QX, United Kingdom

[4]Department of Radiation Science and Technology, Delft University of Technology, Mekelweg 15, 2629 JB Delft, The Netherlands

[a]cioannidou@tudelft.nl, [b]Z.ArechabaletaGuenechea@tudelft.nl, [c]arjan.rijkenberg@tatasteel.com, [d]robert.dalgliesh@stfc.ac.uk, [e]A.A.vanWell@tudelft.nl, [f]S.E.Offerman@tudelft.nl
[§]current address: Tecnalia Research & Innovation, Geldo, Building 700, 48160 Derio, Spain
email: zaloa.arechabaleta@tecnalia.com

Keywords: Small-Angle Neutron Scattering, micro-alloyed steels, precipitation kinetics, Vanadium Carbides, phase transformation, Transmission Electron Microscopy, Scanning Electron Microscopy, Inductively Coupled Plasma Optical Emission Spectroscopy

Abstract. Nano-steels are used in automotive applications to accomplish resource-efficiency while providing high-tech properties. Quantitative data and further understanding on the precipitation kinetics in Nano-steels can contribute to fulfil this goal. Small-Angle Neutron Scattering measurements are performed on a Fe-C-Mn-V steel, previously heat-treated in a dilatometer at 650^{o}C for several holding times from seconds to 10 hours. The evolution of the precipitate volume fraction, size distribution and number density is calculated by fitting the experimental Small-Angle Neutron Scattering curves. The effect of phase transformation on precipitation kinetics is also discussed. Complementary Transmission Electron Microscopy, Scanning Electron Microscopy and Inductively Coupled Plasma Optical Emission Spectroscopy measurements are performed to support the Small-Angle Neutron Scattering data analysis.

Introduction

The automotive industry is continuously looking for opportunities to improve fuel economy and to reduce steel consumption in order to meet the European Union demand for resource efficiency [1]. Steel consumption and CO_2-emissions can be reduced with the use of Nano-steels, developed for light-weight automotive applications. Nano-steels are a new generation of Advanced High Strength Steels (AHSS), that can provide a combination of properties such as high strength, ductility and hole-expansion capacity, which make them highly suitable for demanding automotive applications [2-4]. They consist of a soft ferritic matrix strengthened by nanometer-sized precipitates. Considerable additions of micro-alloying elements such as Vanadium (V), Niobium (Nb), Molybdenum (Mo) and Titanium (Ti) are included in Nano-steels to reach high levels of precipitation strengthening. The key challenge in the design of Nano-steels is to explore options for suitable alloys with reduced amounts of micro-alloying elements and critical raw materials, while maintaining the excellent mechanical properties characteristic for these steels. For this purpose, further knowledge concerning the role of these micro-alloying elements on the precipitation kinetics is required.

Small-Angle Neutron Scattering (SANS) is a powerful tool for studying the precipitation kinetics in steels [5-9]. SANS is used to measure the volume fraction, size distribution and number density of precipitates having dimensions in the nanometer range [10]. The SANS technique has

attracted a lot of interest in this field of research during the last years, because of its ability to provide quantitative data over a large bulk sample volume.

SANS data analysis requires the use of mathematical models that transform the scattering data from the reciprocal space to the real space microstructural parameters [10,11]. In order to interpret the SANS measurements, a suite of complementary microstructural characterization techniques is necessary, which often involves techniques [5-9] such as Transmission Electron Microscopy (TEM), Scanning Electron Microscopy (SEM) and Atom Probe Tomography (APT).

Vanadium is one of the micro-alloying elements used in Nano-steels to achieve strong precipitation strengthening [8,12,13]. The aim of this research is to determine the VC-precipitation kinetics during isothermal annealing at 650^{o}C in a model alloy related to a Nano-steel of interest. SEM, TEM and Inductively Coupled Plasma Optical Emission Spectroscopy (ICP-OES) investigations provide complementary information and confirm the validity of the SANS results.

Experimental

The chemical composition of the alloy is 0.135C-0.013Si-1.83Mn-0.008Al-0.001N-0.0007Ti-0.57V (wt.%) with the balance being iron. The steel is produced by Tata Steel IJmuiden and delivered as a 3mm-thick hot-rolled plate. It is designed to reach an approximate 1% precipitate volume fraction.

A DIL-805 A/D dilatometer (Bähr-Thermoanalysis GmbH) is used for applying heat-treatments to the steel specimens and study the phase transformation kinetics. Plate-shaped samples of dimensions 14x10x1mm^3 (length x width x thickness), machined from the middle of the as-delivered plates, are heated up through inductive heating while Helium gas is used for cooling. The thermal cycle conducted in the dilatometer is the following: the samples are initially heated to 1100ºC in the austenitic region and held there for 15 minutes. This temperature is calculated by Thermo-Calc [14] as the temperature at which all precipitates are dissolved plus an additional 50ºC. After soaking, one sample is directly quenched to room temperature. It is used later as reference as there are no nano-precipitates expected in it. The rest of the samples are quenched to 650ºC, where an isothermal annealing is applied for different holding times from seconds to up to 10h, followed by rapid quenching to room temperature.

SANS experiments are performed at room temperature in the LARMOR Instrument at ISIS Neutron Scattering Centre (STFC Rutherford Appleton Laboratory, United Kingdom). Samples of 10x10x1mm^3 are measured, machined from the specimens previously treated in the dilatometer. For all the measurements, a neutron beam of 7x7mm^2 and a wavelength range of 0.09-1.33nm are used. Measurements corresponding to wavelengths smaller than 0.42nm are not considered in order to avoid Bragg scattering. This leads to a measured scattering intensity in the scattering vector Q-range of $0.04 \leq Q \leq 1.05 nm^{-1}$. A transversal magnetic field of 1.65T perpendicular to the neutron beam is applied, necessary to reach magnetic saturation and prevent scattering from magnetic domains. The magnetic field is generated by a 3473-70 GMW electromagnet. The exposure time to the neutron beam is up to 35 minutes. A ^{3}He tube array-detector with 8x8mm^2 pixel size and dimension of 600x600mm^2 is used with a sample-to-detector distance of 4.3m. The neutron scattering data reduction is performed by using the Mantid software [15].

SEM analysis is conducted to reveal the microstructure of the dilatometry-treated specimens, using a JEOL JSM 6500F microscope. The specimens are prepared for SEM following the standard metallographic sample preparation procedure of grinding, polishing, and finally etching with 2% Nital (2% nitric acid in ethanol).

The ICP-OES technique is used, for comparison to SANS, to calculate the precipitate volume fraction evolution as well. At first, the steel matrix is dissolved by electrolysis. A filtration step follows, where a nanopore filter with a pore size of 20nm is used to separate the precipitates from the matrix. The filters and the filtrate are then dissolved by microwave stimulation and analyzed separately by ICP-OES.

A JEOL JEM-2200FS Transmission Electron Microscope with a resolution of 1.3Å, operating at 200kV is used to identify the shape and size of the precipitates. The dilatometry heat-treated samples are mechanically thinned to 100μm and disks of a diameter of 3mm are punched out from the thin foils. Afterwards, the disks are electro-polished in a twin-jet Struers Tenupol-3 electro-polishing setup, at 19V with a pump flow rate of 12 at 20°C. The electrolyte solution used consists of 5% perchloric acid ($HClO_4$) and 95% acetic acid (CH_3COOH). During the TEM measurements, the imaging is carried out in the scanning mode (STEM) of the instrument and the images are analyzed using the Gatan Digital Micrograph software.

SANS Data Interpretation

In a SANS experiment, the scattering intensity is a function of the scattering vector, $\boldsymbol{Q}$, and consists of two terms due to the two types of interaction between neutrons and matter, the nuclear and the magnetic. The macroscopic differential scattering cross-section, $d\Sigma/d\Omega$, is deduced from the scattering intensity by considering the neutron flux, the sample and the detector characteristics [10,16]. The $d\Sigma/d\Omega$ of a sample magnetized by an external magnetic field is given by [10]:

$$\left(\frac{d\Sigma}{d\Omega}\right)(Q)=\left(\frac{d\Sigma}{d\Omega}\right)_{NUC}(Q)+\left(\frac{d\Sigma}{d\Omega}\right)_{MAG}(Q)\cdot\sin^2 a \tag{1}$$

In Eq. 1, the $(d\Sigma/d\Omega)_{NUC}$ and $(d\Sigma/d\Omega)_{MAG}$ terms are the nuclear and magnetic differential scattering cross-sections, respectively, and α is the angle between the external magnetic field direction and the scattering vector, $\boldsymbol{Q}$. The result of a SANS experiment is a 2D scattering pattern. The 2D raw data is transformed to 1D data of $d\Sigma/d\Omega$ versus Q. For a sample that is magnetically saturated, the scattering intensity measured perpendicular to the applied external magnetic field gives the sum of nuclear and magnetic contributions, whereas the one parallel to the field gives the nuclear contribution [10,17]. The $(d\Sigma/d\Omega)_{NUC}$ is calculated by radial integration of the scattering pattern using two 30-degrees sectors parallel to the applied magnetic field and the $(d\Sigma/d\Omega)_{NUC}+(d\Sigma/d\Omega)_{MAG}$ using sectors perpendicular to it. The pure $(d\Sigma/d\Omega)_{MAG}$ component is then calculated after subtracting the nuclear component from the total measured intensity perpendicular to the magnetic field. Analysis of the differential scattering cross-section, either nuclear or magnetic, gives information for the scattering particles. In the present work, we analyze the nuclear scattering cross section and obtain information about the VC-precipitates in the steel matrix.

The origin of the nuclear scattering is the different chemical composition of the precipitates and the matrix. In a dilute system consisting of precipitates surrounded by a homogenous matrix, the nuclear differential scattering cross section is described by the equation [16]:

$$\left(\frac{d\Sigma}{d\Omega}\right)_{NUC}(Q)=\left(\Delta\rho_{NUC}\right)^2\int D_N(R)\cdot V^2(R)\cdot P^2(Q,R)\,dR \tag{2}$$

In Eq. 2, $\Delta\rho_{NUC}$ is the nuclear contrast, i.e., the difference in nuclear scattering length density, ρ, between the matrix and the precipitates and is given by:

$$\Delta\rho_{NUC}=\rho_{Fe}-\rho_{VC}\cong N_o^{Fe}b_c^{Fe}-N_o^{VC}b_c^{VC} \tag{3}$$

N_o is the number density, calculated for Fe and VC considering their bulk density, ρ_m, and their molecular weight, M:

$$N_o=N_A\cdot\rho_m/M \tag{4}$$

and b_c is the coherent scattering length. In Eq. 2, R is the precipitate radius, $V(R)$ is the precipitate volume, $D_N(R)$ is the precipitate log-normal size number distribution and $P(Q,R)$ is the form factor that is related to the precipitate shape that we assume to be spherical. $D_N(R)$ equals to:

$$D_N(R) = \frac{N_p}{R\sigma\sqrt{2\pi}} \exp\left\{-\frac{\left[\ln(R) - \ln(R_m)\right]^2}{2\sigma^2}\right\} \quad (5)$$

where N_p is the precipitate number density, σ is the standard deviation of the size distribution and R_m is the mean precipitate radius. Integration of $D_N(R)$ gives the precipitate number density. The precipitate volume distribution can be then calculated using the equation $D_V(R) = D_N(R) \cdot V(R)$ and its integral results in the precipitate volume fraction, f_V.

The volume fraction of the precipitates can also be calculated by integrating the Q^2 $(d\Sigma/d\Omega)_{NUC}$ curve (Kratky Plot). For a dual-phase system, the area $Q_{o,NUC}$ below the Q^2 $(d\Sigma/d\Omega)_{NUC}$ plot is [10]:

$$Q_{o,NUC} = \int_0^\infty Q^2 \left(\frac{d\Sigma}{d\Omega}\right)_{NUC} dQ = 2\pi^2 \left(\Delta\rho_{NUC}\right)^2 f_V \left(1 - f_V\right) \quad (6)$$

In steels, the precipitate volume fraction is normally very low, thus, Eq. 6 can be simplified to:

$$f_V \cong \frac{Q_{o,NUC}}{2\pi^2 \left(\Delta\rho_{NUC}\right)^2} \quad (7)$$

Results and Discussion

The phase transformation effect. The purpose of this paper is to follow the precipitation kinetics during the isothermal holding at 650°C for up to 10 hours. However, apart from precipitation, phase transformation also takes place during annealing, affecting the neutron scattering intensity results directly (different phases interact differently with neutrons) and indirectly through its effect on the precipitation kinetics. To disentangle these phenomena, the phase transformation from austenite to ferrite is also studied.

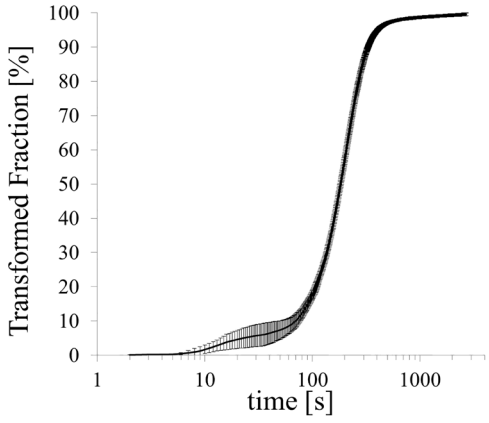

Fig. 1 Amount of phase fraction transformed during annealing at 650°C.

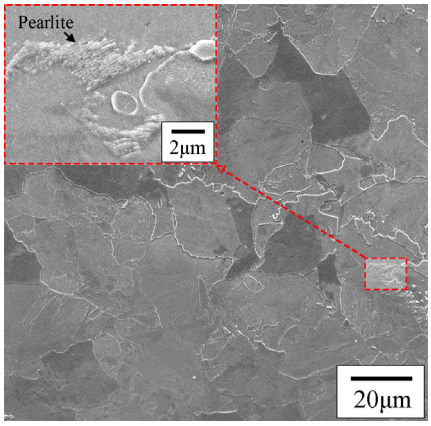

Fig. 2 SEM micrograph of the microstructure of the specimen held for 7min at 650°C.

The phase transformation kinetics is studied by measuring the thermal dilatation of the samples that are quenched to room temperature after following the thermal cycle in the dilatometer described above. The amount of phase fraction transformed during annealing at 650°C is shown in Fig. 1 as a function of annealing time. It is calculated that, after 2min of isothermal holding at 650°C, about 24% of the initial austenite is transformed, while after 20min, about 99% is transformed as shown in Fig. 1. Consequently, the microstructure of the samples annealed for times longer than 20min consists mainly of ferrite. For shorter times, the microstructure consists of ferrite

and austenite at 650°C, and therefore of ferrite and martensite (quenched austenite) at room temperature. As isothermal annealing proceeds, the volume fraction of martensite is decreasing while the one of ferrite is increasing.

SEM characterization of all samples shows the formation of ferrite and martensite, and locally of a small amount of a pearlite-structure (ferrite and cementite). The formation of the pearlite starts at around 1min of annealing. An example of the locally observed pearlite is shown in Fig. 2.

Precipitation Kinetics. In order to study the VC precipitation kinetics individually by SANS, it is necessary to subtract the background signal that comes from the dislocations in the martensite and from the cementite. The SANS measurements are performed at room temperature on the samples treated in the dilatometer, to study the precipitation kinetics during the isothermal holding at 650°C. The SANS nuclear differential scattering cross sections are shown in Fig. 3a. They are obtained by radially integrating the scattering pattern using two 30° sectors parallel to the external magnetic field. Fig. 3a shows the scattering cross sections of the specimens that are annealed for 2, 5, 10, 20 and 45min and for 10h. The scattering cross section of the specimen quenched to room temperature directly from 1100°C is also shown.

Samples annealed for up to 2min give nuclear scattering intensity curves that overlap (except for minor deviations at 2min) and no significant increase in scattering is observed because of precipitation or phase transformation.

Between 2-20min, in the low-Q area (Q<0.2nm^{-1}), the intensity is decreasing. The $(d\Sigma/d\Omega)_{NUC}$ at low Q values is attributed to scattering from large objects like grain boundaries, dislocations [6], and large precipitates. This means that in the time range of 2-20min, while phase transformation is taking place (see Fig. 1 for phase transformation kinetics), the decrease in the scattering intensity in the low Q area is a result of the decrease of the dislocation density (because of the decrease in phase fraction of martensite that has a high dislocation density, Fig. 1). For higher Q values, from 2-20min, an increase in the $(d\Sigma/d\Omega)_{NUC}$ is observed. This strongly indicates the dominant scattering effect of small precipitates in the high Q range.

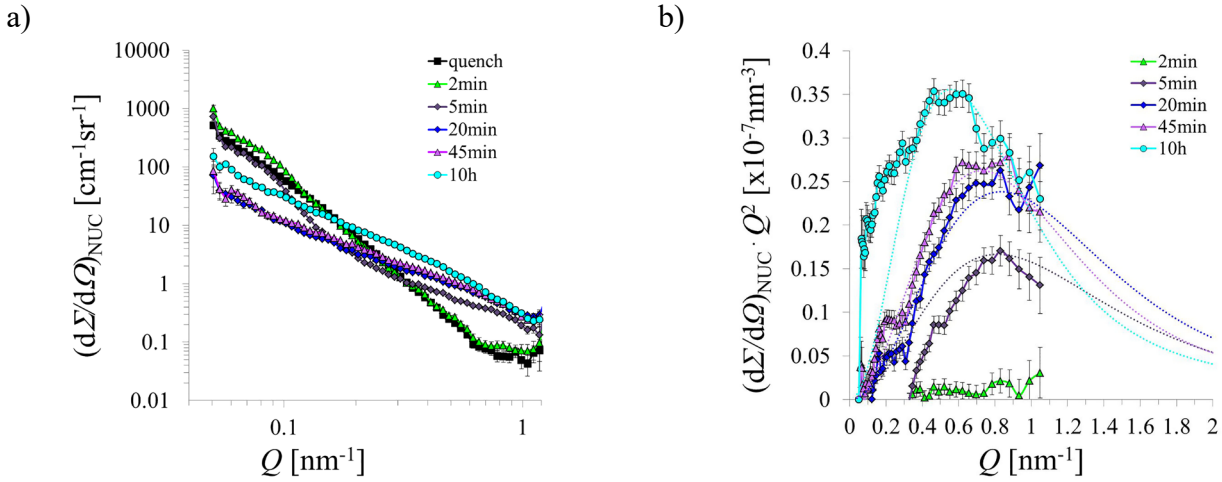

Fig. 3 a) Time evolution of the $(d\Sigma/d\Omega)_{NUC}$ as a function of Q measured at room temperature after annealing at 650°C for up to 10h. Only scattering from the samples heat treated under the most representative conditions is plotted. b) Calculated time evolution of Q^2 $(d\Sigma/d\Omega)_{NUC}$ vs. Q (data points), corresponding to Fig. 3a, after background subtraction. The thin dotted lines represent the theoretical Q^2 $(d\Sigma/d\Omega)_{NUC}$ curves based on Eq. 2 and the fitting parameters. Deviations in the low Q range are most probably related to difficulties in the background subtraction of contributions to the scattering intensity, not coming from the precipitates.

For annealing times longer than 20min, additional scattering is observed through the whole Q range. After 20min, in the low Q range and since the phase transformation has almost been completed, the major contribution to the signal is coming from pearlite (a large precipitate) and

from the large VC precipitates that have grown or coarsened during annealing. A smaller increase in the signal in the high Q area is also measured, coming from smaller precipitates.

In order to study the precipitate volume fraction evolution during annealing, it is important to isolate the VC precipitates' scattering contribution to the signal. In Fig. 3b, the Q^2 $(d\Sigma/d\Omega)_{NUC}$ curves are presented after subtraction of the background signal, which includes the dislocations and the cementite contribution to scattering. The most representative heat-treatment conditions are presented for the sake of simplicity.

A gradual increase in the Q^2 $(d\Sigma/d\Omega)_{NUC}$ curves in Fig. 3b with annealing time is observed. As the holding time increases, the peak position of the Q^2 $(d\Sigma/d\Omega)_{NUC}$ curves is moving to the low Q area (left), indicating the presence of large precipitates as a result of growth or coarsening.

Quantitative information regarding the precipitation kinetics can be gained by using the model for the precipitation scattering described above (Eq. 1 to Eq. 7). The model is applied to the neutron scattering results of all the samples annealed for different times. The purpose is to obtain the model parameters (R_m, N_p and σ) at each time step of annealing by fitting all the Q^2 $(d\Sigma/d\Omega)_{NUC}$ curves, and thus, determine the precipitation kinetics.

The number density of Fe atoms is $N_o^{Fe} = 84.9nm^{-3}$, calculated using Eq. 4. Assuming that the precipitates are pure VC having a stoichiometric composition (V/C ratio equals to 1), the number density of VC atoms is $N_o^{VC} = 55.1nm^{-3}$ (from Eq. 4). The scattering length of the matrix and the precipitates is: $b_c^{Fe} = 9.45x10^{-15}m$ and $b_c^{VC} = 6.26x10^{-15}m$, respectively, resulting to a $\Delta\rho_{NUC}^2 = 20.8x10^{-8}nm^{-4}$ using Eq. 3. Considering spherical VC precipitates with a radius R, the precipitate volume is then $V(R)=4/3\pi R^3$ and the form factor is $P(Q,R)=3[\sin(QR)-(QR)\cos(QR)]/(QR)^3$ [11,16]. Based on the above, the Q^2 $(d\Sigma/d\Omega)_{NUC}$ curves are fitted by the fit function which a product of Eq. 2 multiplied by Q^2.

It is important to note here the assumptions that we make may introduce a small uncertainty to the results. For the precipitation analysis we consider a stoichiometric chemical composition and a spherical shape for all the precipitates. Moreover, in Eq. 4, the bulk VC density value, $\rho_{m,VC}$, is used for the precipitate atomic number density calculation, which may deviate from the actual density value of the nano-precipitates.

The mean precipitate radius, R_m, and the precipitate number density, N_p, evolution during annealing from 5min to 10h is shown in Fig. 4a and Fig. 4b. The values of R_m and N_p are determined directly from the fitting of the Q^2 $(d\Sigma/d\Omega)_{NUC}$ curves. The fitting model is applied only to the Q^2 $(d\Sigma/d\Omega)_{NUC}$ curves corresponding to annealing times larger than 5min. In the Q^2 $(d\Sigma/d\Omega)_{NUC}$ curves of the samples annealed for less than 2min, no significant changes in the scattering signal are observed because of precipitation (Fig. 3a) and therefore the resulting Q^2 $(d\Sigma/d\Omega)_{NUC}$ curves of these samples are not fitted to the precipitation model. This is due to the effect of phase transformation: Vanadium tends to remain in solid solution in austenite and when some fraction of ferrite is formed after 2min of annealing, the precipitation starts (Fig. 4c). Moreover, when a sufficient volume fraction of ferrite is formed (about 86% after 5min of annealing (dilatometry curve Fig. 1), the precipitation is enhanced (Fig. 4c). This is in agreement to previous studies [12].

As shown in Fig. 4a, the precipitate mean radius, R_m, increases with time due to continuous growth. The precipitate size range is very close to the resolution limit of the SANS technique and the background signal from the dislocations is substantial, which results in the large error bars in Fig. 4a and Fig. 4b.

The initial increase in the precipitate number density N_p (Fig. 4b) till 20min at 650°C, denotes that the continuous formation of new nuclei is the dominant phenomenon in this time range. After 20min, the precipitate number density decreases while annealing, indicating that the coarsening process is taking place. During this process the large precipitates grow at the expense of the smaller ones.

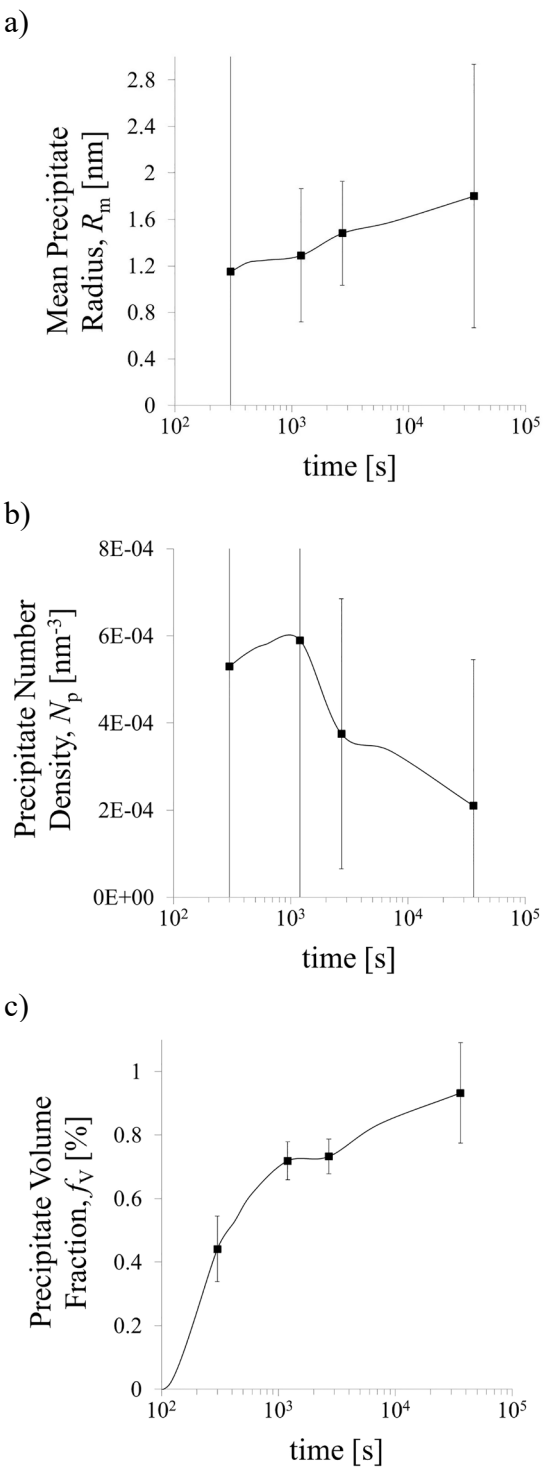

Fig. 4 Precipitate a) mean radius, b) number density and c) volume fraction evolution during annealing at 650°C.

The log-normal precipitate volume distribution ($D_V(R) = D_N(R)V(R)$) of the VC precipitates is plotted in Fig. 5 as a function of the precipitate radius, R, for different isothermal holding times at 650°C. The peak position of the D_V is related to the average precipitate size at that moment of precipitation. From the onset of precipitation till the 20min of annealing, the volume distribution increases with time without a significant shift in the peak position, pointing out the formation of many small nuclei. As the isothermal holding time is increasing, the volume distribution is gradually broadening while its peak is reducing. The peak position is shifting to larger R values because the precipitate coarsening effect is becoming stronger.

The precipitate volume fraction evolution, f_V, can be calculated by integrating the area under the $Q^2(d\Sigma/d\Omega)_{NUC}$ plots using (Eq. 7). It is important to note here that the Q range of the experimental data is $0.04 \leq Q \leq 1.05 nm^{-1}$ (Fig. 3a), restricting the direct Q range of observation. This would lead to smaller f_V values than the real ones as a result of the limited Q area that is measured.

In order to overcome this obstacle, for the total volume fraction calculation, the total area below the $Q^2(d\Sigma/d\Omega)_{NUC}$ curves, $Q_{o,NUC}$, is taken as the sum of $Q_{o,1,NUC}+Q_{o,2,NUC}$. $Q_{o,1,NUC}$ corresponds to the area below the $Q^2(d\Sigma/d\Omega)_{NUC}$ experimental calculated plot for the Q range of $0.04 \leq Q \leq 1.05 nm^{-1}$. $Q_{o,2,NUC}$ is the area below the theoretical $Q^2(d\Sigma/d\Omega)_{NUC}$ for the Q range of $1.05 \leq Q \leq 2 nm^{-1}$, calculated by multiplying Eq. 2 by Q^2 and using the R_m, N_p and σ values from the fitting of the experimental $Q^2(d\Sigma/d\Omega)_{NUC}$ results.

The evolution of the precipitate volume fraction during annealing at 650°C, is shown in Fig. 4c. Before 2min, no significant amount of precipitates is detected, whereas precipitation is enhanced at longer times reaching a maximum value of 0.93±0.16% after 10h of annealing. The Thermoc-Calc software (database TCFE9) [14], gives an equilibrium volume fraction of 1.09%, concluding that almost all of the Vanadium is in form of precipitates. The continuous increase in volume fraction after 20min when the number density of the precipitates is decreasing confirms the fact that the precipitates undergo coarsening.

Complementary ICP-OES and TEM measurements. For comparison to the SANS results, the amount of Vanadium that has precipitated during annealing is measured by means of ICP-OES. The volume fraction of the VC precipitates is then calculated as a function of the measured amount of V in the precipitates, assuming stoichiometric VC precipitates. Two samples corresponding to two different annealing conditions, are analyzed by ICP-OES. The derived f_V is listed in Table 1. Comparison between the ICP-OES and the SANS f_V results shows no significant deviations, confirming the validity our SANS data analysis.

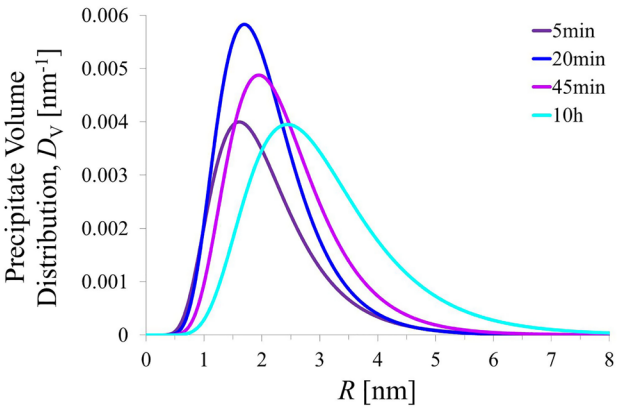

Fig. 5 Log-normal volume distribution, D_V, of the VC precipitates during annealing at 650°C for up to 10h. The curves are based on the R_m, N_p and σ values resulted from the fitting of the experimental $Q^2\,(d\Sigma/d\Omega)_{NUC}$ results.

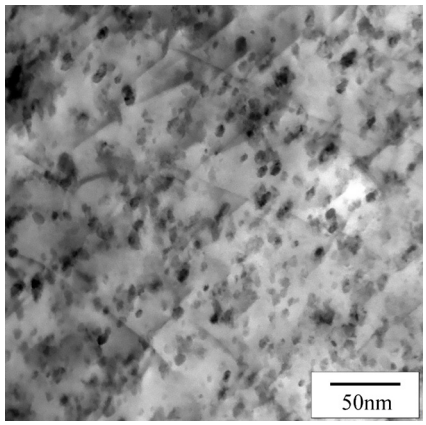

Fig. 6 TEM micrograph showing the precipitates in the ferritic matrix of the specimen annealed at 650°C for 20min.

Additional information from TEM is proven very useful as well. TEM is used here to capture the precipitates and derive valuable information that can contribute to the SANS precipitation kinetics analysis. Fig. 6 is a bright-field TEM image of the sample annealed at 650°C for 20 minutes and finally quenched to room temperature. The precipitates are the randomly distributed black spots that are surrounded by the grey ferritic matrix. The micrograph shows spherical or slightly ellipsoidal precipitates, supporting the assumption of spherical precipitates used in SANS analysis. The precipitates here have an average radius of ~1.1nm, very close to what is calculated by SANS for this condition (R_m = 1.3 ± 0.6nm).

Table 1 Precipitate Volume Fraction, f_V [%], comparison between ICP-OES and SANS

Annealing time	ICP-OES	SANS
5min	0.47 ± 0.05	0.44 ± 0.10
10h	0.75 ± 0.08	0.93 ± 0.16

Conclusions

SANS measurements performed at room temperature are used to characterize the precipitation kinetics of VC in an Fe-C-Mn-V Nano-steel during annealing at 650°C for up to 10 hours. The evolution of the precipitate mean radius, volume fraction, size distribution and number density is determined by fitting the experimental nuclear SANS data to a log-normal, spherical size distribution for the precipitates. The main conclusions are summarized as following:

- VC-precipitates form with sizes of about 1-2nm during annealing at 650°C. Combining the dilatometry phase transformation analysis to the SANS precipitation kinetics results, it is concluded that VC precipitation starts after the onset of phase transformation, the two phenomena occur simultaneously till the 20min of annealing and precipitation continues to take place after phase transformation completion. The precipitates nucleate, grow and coarsen, thus, their volume fraction increases with annealing time.
- SEM, TEM and ICP-OES techniques provide complementary information, supporting the SANS data and their analysis. Spherical precipitates are observed in TEM with sizes that are in agreement with the SANS measurements. ICP-OES is used to quantify the evolution of the precipitate volume fraction, giving f_V results consistent with the SANS f_V results.

Acknowledgements

This work is part of the "Nano-Steel" Project, which is funded by the Dutch Technology Foundation STW (project 14307) and by Tata Steel through its contribution to the Materials innovation institute M2i (project S41.5.14548). The authors wish to thank N. Geerlofs (TUDelft) for his contribution to the dilatometry treatments and V. Bliznuk (UGent) for the TEM measurements.

References

[1] European Commission, A resource-efficient Europe - Flagship initiative under the Europe 2020 Strategy, COM 21 (2011).

[2] WO2013167572 (A1), Automotive chassis part made from high strength formable hot rolled steel sheet, Tata Steel Europe.

[3] K. Seto et al., Hot rolled high strength steels for suspension and chassis parts "NanoHiten" and "BHT" steel, JFE Technical Report No. 10 2007.

[4] A. Rijkenberg et al., Advanced high stretch-flange formability steels for chassis & suspension applications, Conference proceedings of the 4th International Conference on Steels in Cars and Trucks (SCT2014) Germany, 2014, pp. 426.

[5] N.H. van Dijk et al., High Temperature SANS Experiments on Nb(C,N) and MnS Precipitates in HSLA Steel, Metallurgical and Materials Transactions A 33 (2002) 1883-1891.

[6] S.M. He et al., In situ determination of aging precipitation in deformed Fe-Cu and Fe-Cu-B-N alloys by time-resolved small-angle neutron scattering, Phys. Rev. B 82 (2010) 174111 1-14.

[7] S. Zhang et al., Defect-induced Au precipitation in Fe–Au and Fe–Au–B–N alloys studied by in situ small-angle neutron scattering, Acta Materialia 61 (2013) 7009–7019.

[8] Y.Q. Wang et al., Investigating nano-precipitation in a V-containing HSLA steel using small angle neutron scattering, Acta Materialia 145 (2018) 84-96.

[9] F. Perrard et al., A small-angle neutron scattering study of fine-scale NbC precipitation kinetics in the α-Fe-Nb-C system, J. Appl. Cryst. 39 (2006) 473-482.

[10] A. Wiedenmann, Small Angle Scattering Investigations of Magnetic Nanostructures, in T. Chatterji (Ed.), Neutron Scattering from Magnetic Materials, Elsevier, 2006, pp. 473-519.

[11] L.A. Feigin, Structure Analysis by small-angle X-ray and neutron scattering, New York, 1987.

[12] R. Lagneborg et al., The role of Vanadium in microalloyed steels, Scandinavian Journal of Metallurgy 28 (1999) 186-242.

[13] T.N. Baker, Processes, microstructure and properties of Vanadium microalloyed steels, Materials Science and Technology 25 (2009) 9 1083-1107.

[14] J.O. Andersson et al., THERMO-CALC and DICTRA, Computational Tools For Materials Science, Calphad 26 (2002) 2 273-312.

[15] O. Arnold et al., Mantid-Data analysis and visualization package for neutron scattering and μ SR experiments, Nuclear Instruments and Methods in Physics Research A 764 (2014) 156-166.

[16] T. Narayanan, Synchrotron Small-Angle X-Ray Scattering, in R. Borsali, R. Pecora (Eds.), Soft-Matter Characterization, Springer, 2008, pp. 899-948.

[17] D.S. Sivia, Elementary Scattering Theory for X-ray & Neutron Users, O.U.P., 2011, pp. 74-75.